Since January 2020 Elsevier has created a COVID-19 resource centre with free information in English and Mandarin on the novel coronavirus COVID-19. The COVID-19 resource centre is hosted on Elsevier Connect, the company's public news and information website.

Materials Today Chemistry 24 (2022) 100817

Contents lists available at ScienceDirect

Materials Today Chemistry

journal homepage: www.journals.elsevier.com/materials-today-chemistry/

Development of polypyrrole (nano)structures decorated with gold nanoparticles toward immunosensing for COVID-19 serological diagnosis

B.M. Hryniewicz [a, 1], J. Volpe [b, 1], L. Bach-Toledo [a], K.C. Kurpel [c], A.E. Deller [a], A.L. Soares [a], J.M. Nardin [d], L.F. Marchesi [a, e], F.F. Simas [c], C.C. Oliveira [c], L. Huergo [f], D.E.P. Souto [b, **], M. Vidotti [a, *]

[a] Grupo de Pesquisa Em Macromoléculas e Interfaces, Departamento de Química, Universidade Federal Do Paraná (UFPR), 81531-980, Curitiba, PR, Brazil
[b] Laboratório de Espectrometria, Sensores e Biossensores, Departamento de Química, Universidade Federal Do Paraná (UFPR), 81531-980, Curitiba, PR, Brazil
[c] Laboratory of Inflammatory and Neoplastic Cells, Cell Biology Department, Section of Biological Sciences - Universidade Federal Do Paraná (UFPR), 81531-980, Curitiba, PR, Brazil
[d] Hospital Erasto Gaertner, 81520-290, Curitiba, PR, Brazil
[e] Universidade Tecnológica Federal Do Paraná, Av. Monteiro Lobato S/n Km 04, CEP, 84016-210, Ponta Grossa, PR, Brazil
[f] Setor Litoral, Universidade Federal Do Paraná (UFPR), 83260-000, Matinhos, PR, Brazil

ARTICLE INFO

Article history:
Received 23 October 2021
Received in revised form
10 January 2022
Accepted 27 January 2022
Available online 7 February 2022

Keywords:
Impedimetric biosensor
Immunosensor
COVID-19
Polypyrrole modified electrode
Polypyrrole nanotubes
Gold nanoparticles

ABSTRACT

The rapid and reliable detection of severe acute respiratory syndrome coronavirus 2 (SARS-CoV-2) seroconversion in humans is crucial for suitable infection control. In this sense, many studies have focused on increasing the sensibility, lowering the detection limits and minimizing false negative/positive results. Thus, biosensors based on nanoarchitectures of conducting polymers are promising alternatives to more traditional materials since they can hold improved surface area, higher electrical conductivity and electrochemical activity. In this work, we reported the analytical comparison of two different conducting polymers morphologies for the development of an impedimetric biosensor to monitor SARS-CoV-2 seroconversion in humans. Biosensors based on polypyrrole (PPy), synthesized in both globular and nanotubular (NT) morphology, and gold nanoparticles are reported, using a self-assembly monolayer of 3-mercaptopropionic acid and covalently linked SARS-CoV-2 Nucleocapsid protein. First, the novel hybrid materials were characterized by electron microscopy and electrochemical measurements, and the biosensor step-by-step construction was characterized by electrochemical and spectroscopic techniques. As a proof of concept, the biosensor was used for the impedimetric detection of anti-SARS-CoV-2 Nucleocapsid protein monoclonal antibodies. The results showed a linear response for different antibody concentrations, good sensibility and possibility to quantify 7.442 and 0.4 ng/mL of monoclonal antibody for PPy in the globular and NT morphology, respectively. The PPy-NTs biosensor was able to discriminate serum obtained from COVID-19 positive versus negative clinical samples and is a promising tool for COVID-19 immunodiagnostic, which can contribute to further studies concerning rapid, efficient, and reliable detections.

1. Introduction

The coronavirus disease (COVID-19) started in late 2019 in Wuhan, China, caused by the new virus called severe acute respiratory syndrome coronavirus 2 (SARS-CoV-2) and was rapidly transmitted through humans mostly via saliva droplets and nasal discharges from infected people. COVID-19 was classified as a global pandemic by the World Health Organization (WHO) and

** Corresponding author.
* Corresponding author.
E-mail addresses: denio.souto@ufpr.br (D.E.P. Souto), mvidotti@ufpr.br (M. Vidotti).
[1] These authors contributed equally to this study.

https://doi.org/10.1016/j.mtchem.2022.100817
2468-5194/

presents as primary symptoms fever, cough, difficulty breathing, and so on. However, some patients remain asymptomatic, which raises the potential of the silent sparseness of the disease [1,2].

The screening of new SARS-CoV-2 contaminated individuals is crucial, especially in the absence of a cure, for better isolation measures, infection control, treatment, and other epidemiological considerations [2,3]. Pokhrel et al. have shown that lower mortality of COVID-19 can be related to early detection of infections and consequent patient isolation, comparing five countries with similar age distribution and hospital resources.[3] Nowadays, the most common tests available are the lateral flow immunochromatographic strip, real-time reverse transcriptase-polymerase chain reaction (RT-PCR), enzyme-linked immunosorbent assay, and chemiluminescence assay. However, each of the current options may provide qualities and defects that must be considered individually by case [4]. The interest of diagnostics mainly remains in techniques that supply mobility, agility in the result, ease of sampling, high detectability and minimize false positives and negatives responses. Biosensors offer an alternative sensitive method that may facilitate the diagnosis of SARS-CoV-2 infection [5].

Different materials can be used to fabricate biosensors, such as conducting polymers (CPs), molecularly imprinted polymers, metal and metal oxides nanoparticles, carbon-based materials, quantum dots, among others [6,7]. CPs presents along their chemical structures a π-conjugated system with alternating double and single bonds, responsible for the improved movement of electrons, attributing conductivity to these materials. The use in electrochemical biosensors is compelling because of its biocompatibility, possibility of simple tuning its properties by doping and de-doping process, and the ability to couple it with several materials (gold nanoparticles, metal oxides, and so on) [8,9]. The performance of CPs-based electrochemical biosensors relies on changes in their electrical properties, being highly dependent on their shape, size, structure, conductivity, and morphology [10,11].

Among the different electrochemical biosensors, the electrochemical impedance spectroscopy (EIS) ones stand out for the possibility to detect small electrode surface variations, as the biorecognition processes, and the detection in a steady-state situation, being less destructive than other electrochemical methods, as cyclic voltammetry (CV) and differential pulse voltammetry [12]. Usually in this type of biosensor, the charge-transfer resistance (*Rct*) at the electrode/electrolyte interface is measured, being sensitive to macromolecules that are recognized at the electrode surface. Usually, a redox probe is added in the electrolyte for EIS measurements since a *Rct* appearance is resultant of faradaic reactions at electrode/electrolyte interface [13]. However, when CPs are deposited at the electrode surface, the use of a probe becomes unnecessary because CPs themselves suffer from redox reactions and, consequently, have an associated *Rct* [14].

Different polymer morphologies, such as nanoarchitectures, are able to offer material properties improvement, including a higher electroactive area and facilitated charge-transfer process, thus offering higher sensitivity, good recovery and a fast response in sensing applications [8,15]. Also, the association with gold nanoparticles (AuNPs) can improve even more stability, biocompatibility, sensitivity, and selectivity of the CPs, making this strategy very appealing for new COVID-19 biosensors applied as new tools for diagnosis [11,16].

Polypyrrole (PPy) is a well-known CP that provides a high conductivity, fair redox properties, stability, facility of synthesis, and electroactivity in phosphate buffer (pH 7.4) [17–20]. In biosensors, PPy have been evaluated in different nanocomposites and morphologies due to its promising properties in this area, achieving excellent analytical parameters, such as chitosan/PPy-NTs(polypyrrole nanotubes)/AuNPs [18], over-oxidized PPy-NTs/AuNPs [21], PPy polymer containing epoxy active side group [22], and PPy/reduced graphene oxide [23].

In the present work, two different morphologies of PPy (globular and nanotubular), both modified with gold nanoparticles, were synthesized in stainless steel mesh electrodes. This affordable substrate allows the final product to be relatively cheap, flexible, and disposable. Firstly, the materials synthesis was characterized via scanning electron microscopy (SEM), electrochemical and spectroscopical techniques, such as EIS and CV. Later, the modified electrodes were applied to build an immunosensor for SARS-CoV-2 antibodies detection by covalent immobilization of SARS-CoV-2 Nucleocapsid protein (N) via thiol self-assembled monolayers (SAMs) methodology [24–26], and each of the steps were characterized via EIS, CV, and Fourier-transform infrared spectroscopy. Finally, the materials were analytically compared by its response to purified monoclonal antibodies to the N protein and tested to identify infections in real samples.

2. Experimental

2.1. Chemical and materials

All solutions were prepared using ultrapure water (R = 18.2MΩ cm in 25 °C, ElgaLab system). For the modified electrode preparation, all the following reagents used were of analytical grade: pyrrole (98%), poly(sodium-4-styrene sulfonate), gold (III) chloride hydrate ($HAuCl_4 \cdot 3H_2O$), methyl orange (MO), ethylenediaminetetraacetic acid, potassium nitrate (KNO_3), sodium hydrogen phosphate (Na_2HPO_4), potassium chloride (KCl), potassium hydroxide (KOH) were purchased from Sigma-Aldrich Chemical (St. Louis, MO, USA), sodium sulfite (Na_2SO_3), potassium dihydrogen phosphate (KH_2PO_4), and nitric acid (HNO_3) were purchased from Synth (Diadema, SP, Brazil). The monomer (Pyrrole) was distilled under low pressure and bubbled with N_2 stream and kept in the refrigerator (−18 °C) until its use.

For the biosensor experiments, 3-mercaptopropionic acid (MPA), N-hydroxysuccinimide (NHS), N- (3-dimethylaminopropyl) -N-ethylcarbodiimide (EDC) and bovine serum albumin (BSA) (heat shock fraction, pH 7) were purchased from Sigma-Aldrich Chemical (St. Louis, MO, USA).

The recombinant Nucleocapsid protein (N-protein) expression and purification was carried according to procedure present in the study by Huergo et al. [27]. The monoclonal antibody against SARS-CoV-2 Nucleocapsid protein was obtained from FAPON Biotech (Dongguan, China).

The human serum samples were collected from COVID-19 patients at Hospital Erasto Gaertner in Curitiba, Brazil. Positive cases were confirmed through SARS-CoV-2 RNA detection by qRT-PCR from nasopharyngeal swabs samples. The negative samples were collected from healthy donors. All the samples were acquired with informed consent. All the methods were performed in accordance with the relevant guidelines and regulation, being approved by the Institutional Ethics Review Board of CEP/HEG (n# 31592620.4.1001.0098).

2.2. PPy electrochemical synthesis and association with AuNPs

The electrochemical procedures were performed in an IviumStat XRe potentiostat, and a Metrohm DropSens STAT-I-400 portable potentiostat. Electropolymerization has been preferred due to its simplicity, speed, and reproducibility. It can be performed in a three-electrode conventional conformation (reference, counter, and working electrodes) in an electrochemical solution simply containing the monomer and a supporting electrolyte, applying a constant potential and monitoring the current over time [28]. The

reference electrode and counter electrode were, respectively, Ag/AgCl/$KCl_{(sat)}$ and a platinum spiral. The working electrode was a steel mesh with an area of 1.2 cm^2, equally divided into four minor electrodes that were later cut to be used as our transducer in the biosensing experiments.

PPy-NTs were synthesized by the methodology previously performed by our group [17]. The electrochemical medium included 50 mmol/L of the monomer pyrrole, 5 mmol/L of MO (as template), and 8 mmol/L of KNO_3 (as supporting electrolyte), and the pH of the solution was adjusted with 1 mol/L HNO_3 to the final pH 2 at 25 °C. The electropolymerization was carried out potentiostatically by applying 0.8 V and monitoring the current over time. To assure the amount of polymer was kept the same between the syntheses, the quantity of PPy-NTs on the working electrode surface was supervised by charge control of 500 mC cm^{-2}.

For the PPy:PSS synthesis, the reaction medium was composed of 50 mmol/L of pyrrole and 14 g/L NaPSS, and carried out based on previous works published elsewhere [29–31]. For the film electropolymerization, it was used a constant potential of 0.8 V with a charge cutoff of 800 mC cm^{-2} to get similar electrochemical performance compared with PPy-NTs modified electrodes.

The same protocol for AuNPs incorporation was performed onto both polymeric morphologies (PPy-NTs and PPy:PSS) of the modified electrodes. The synthetic medium is composed by 1.0 mmol/L $HAuCl_4 \cdot 3H_2O$, 0.17 mol/L K_2HPO_4, 36 mmol/L Na_2SO_3, and 0.48 mmol/L ethylenediaminetetraacetic acid [31]. To prepare this solution, it is important to slowly add the reagents following this order, avoiding gold precipitation. The electrodeposition was carried under potentiostatic conditions, applying a potential of −1.1 V, with charge control of 300 mC cm^{-2}. An schematic representation of the expected final morphologies, nanotubular (PPy-NT/AuNP) and globular (PPy:PSS-AuNP), are present in Fig. 1.

To characterize the synthesis of PPy-NTs/AuNPs and PPy:PSS/AuNPs EIS data were acquired by applying an alternating voltage of 10 mV, in open-circuit potential, in a frequency range from 10 kHz to 0.01 Hz for PPy:PSS and 10 kHz to 0.1 Hz for PPy-NTs. All the EIS and CV measurements were made in 0.1 mol/L phosphate-buffered saline (PBS) (prepared by adding equimolar concentrations of Na_2HPO_4, KH_2PO_4 and KCl). The synthesized materials were also analyzed by SEM, STEM, and energy-dispersive X-ray spectroscopy (EDS) in a TESCAN MIRA3, with SDD of 80 mm^2 detector for EDS. The material was immobilized onto the stubs with carbon stripes. TEM image was acquired in a JEOL JEM 1200EX-II. For STEM and TEM images, the materials were dispersed in ethanol under sonication and drop casted on grids.

2.3. Biosensors construction

For both polymers morphologies, N-Protein covalent immobilization through MPA SAM formation was chosen, for future comparison. Every step for the biosensor construction is described thoroughly below. A scheme representing each step is presented in Fig. 1, illustrating for better understanding the (a) functionalization, (b) activation, (c) immobilization, (d) blocking, and (e) detection. With exception of the activation step (due to its high instability), all the steps were characterized via EIS and Fourier Transform Infrared Spectroscopy – FTIR, plus CV which is included in the Supplementary Information. The FTIR spectra were acquired in a Bruker spectrometer, scanning from 400 to 4,000/cm, 32 scans, with a resolution of 4/cm, in transmission mode.

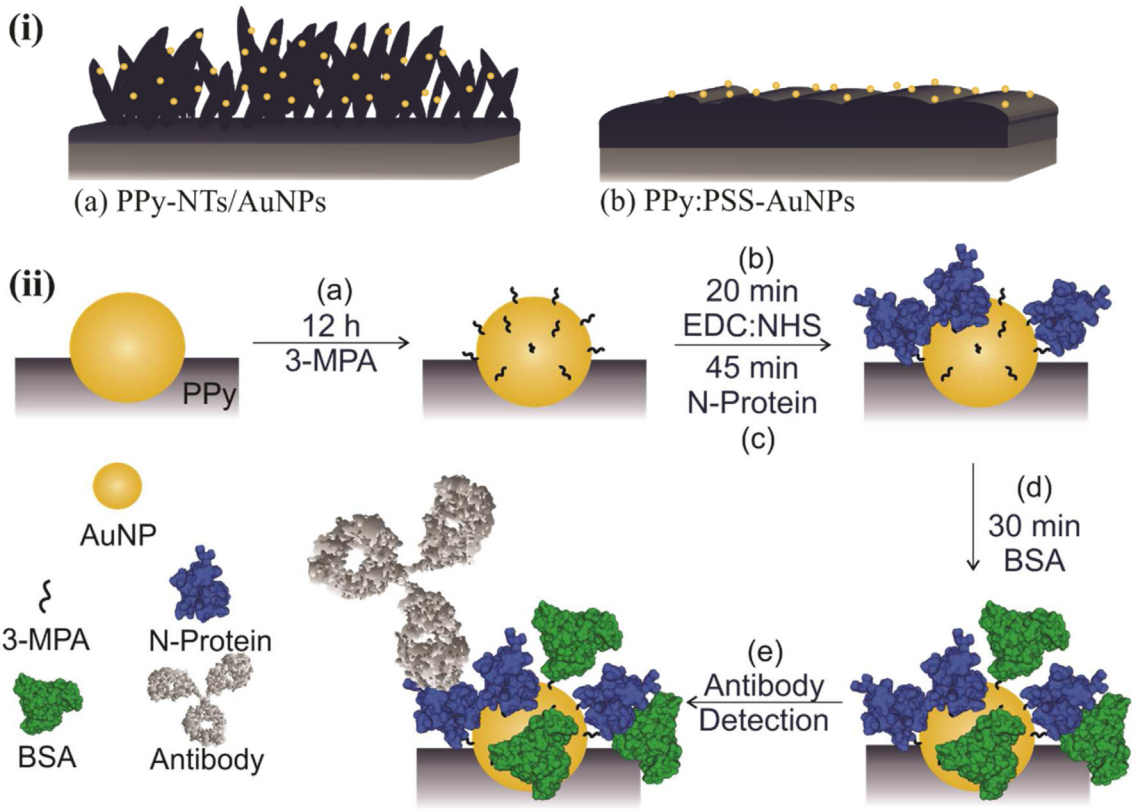

Fig. 1. Schematic representation of (i) expected PPy morphologies: (**a**) nanotubular and (**b**) globular, and (ii) biosensor construction steps for antibody detection. Steps: (**a**) Functionalization though SAM formation, (**b**) activation via EDC:NHS, (**c**) immobilization of N-Protein, (**d**) Blocking via BSA and (**e**) antibody detection. BSA, bovine serum albumin; EDS, energy-dispersive X-ray spectroscopy; NHS, N-hydroxysuccinimide; PPy, polypyrrole; SAM, self-assembly monolayer.

For biosensor construction [16]: (a) Gold nanoparticle surface functionalization was performed by dipping the synthesized electrode into an MPA (1 mmol/L) freshly prepared aqueous solution for at least 12 h. The use of water was due to the high solubility of PPy in ethanol, which could be removed from the electrode surface. After this step, the electrode was carefully washed with water. (b) Then, the terminal carboxylic groups were activated via EDC:NHS (10:15 mmol/L) for 20 min, and prior immobilization of the recognition element, the electrode was carefully washed with PBS pH 7.4 as previously described. (c) Finally, the N-protein was immobilized onto AuNPs surface by dipping the electrode into a solution of the antigen for 45 min. The concentration of the N-Protein (in PBS pH 7.4) used in this step was different for each of the PPy morphologies: 200 ng mL^{-1} for PPy-NTs and 1 μg/mL for PPy:PSS since this last one did not present any significant change in the *Rct* when tested with lower antigen concentrations. After immobilization, the electrode was dipped in a PBS solution for 15 min to assure that the non-strongly linked proteins were washed. (d) To ensure that unbound reactive groups were deactivated and not available for non-specific interactions, the electrode were immersed in 1% BSA solution (freshly prepared in PBS) for 30 min and further washed in PBS for 10 min. After this step, the modified electrode was ready to be exposed to different concentrations of purified antibody solutions and real blood serum samples.

2.4. Biosensors evaluation

PPy:PSS and PPy-NTs were then compared according to their analytical parameters via EIS when their correspondent biosensors were exposed to different concentrations of the purified monoclonal antibody for N-protein (FAPON Biotech). For PPy:PSS, the mAb tested concentrations were 10, 20, 30, 40, 50, and 60 ng/mL, while for PPy-NTs the concentration range were 0.4, 1.0, 2.0, 4.0, 6.0, and 8 ng/mL. The parameter used for the calibration curves construction was *ΔRct*, being this term the difference between the biosensor *Rct* right before its exposure to the analyte solution, and the *Rct* after the correspondent solution containing antibodies to overcome the *Rct* differences between the different constructed electrodes [6]. For detection, the biosensor was previously characterized by EIS, in open-circuit potential, from 10 kHz to 0.1 Hz, applying an alternating voltage of 10 mV (analysis in PBS). Then, it was immersed into the purified antibody solution for 30 min, and it was carefully washed by dipping it in a PBS solution for 5 min prior to EIS analysis. The biosensor was then moved for a clean PBS and the same conditions for EIS were carried out.

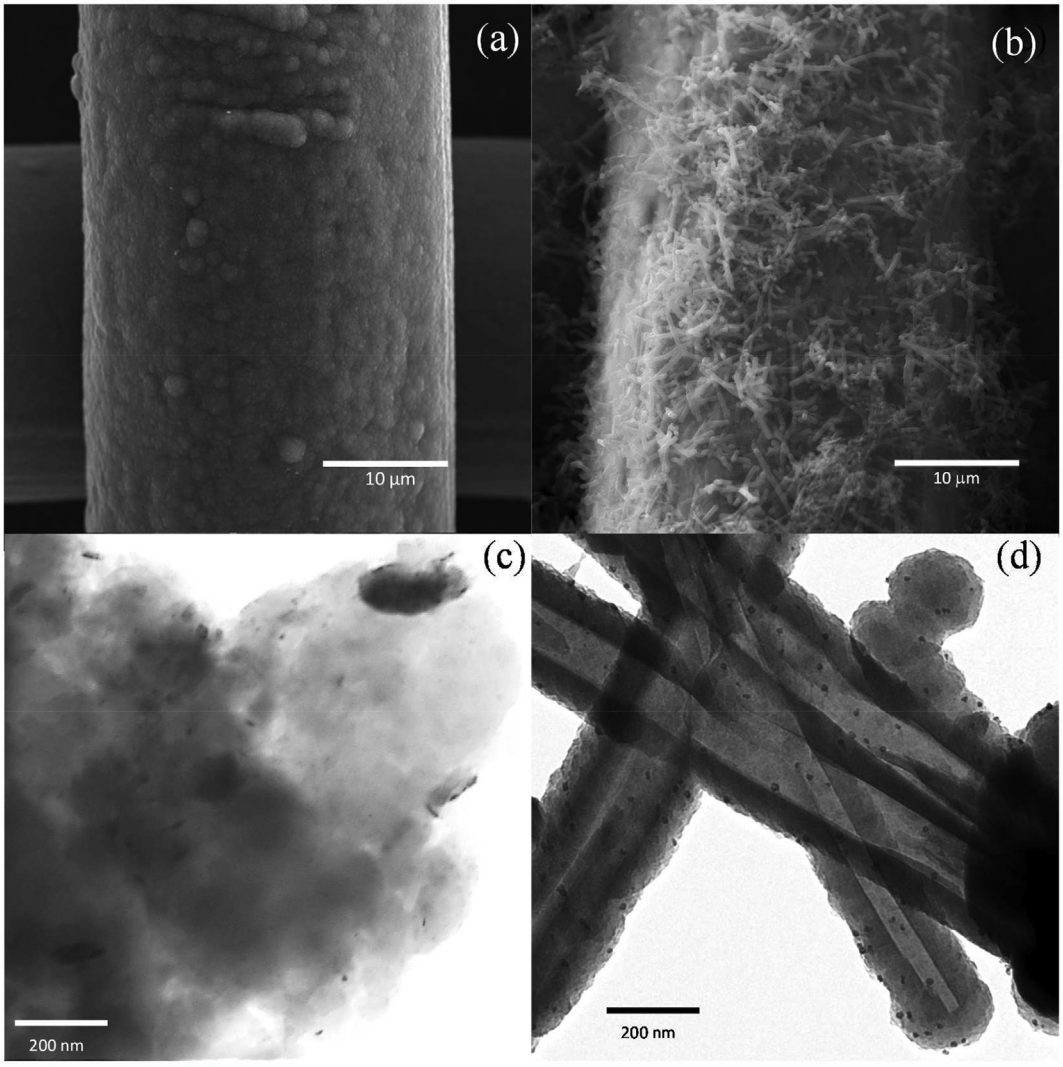

Fig. 2. Representative SEM images of (**a**) PPy:PSS and (**b**) PPy-NTs deposited on stainless-steel mesh. (**c**) STEM image of PPy:PSS and (**d**) TEM image of PPy-NTs. NT, nanotube; PPy, polypyrrole; SEM, scanning electron microscopy; STEM, TEM,

2.5. Detection of SARS-CoV-2 seroconversion in clinical samples

To analyze the biosensor ability to detect antibodies in clinical samples, the PPy-NTs biosensor was exposed to different dilutions (1:40000, 1:20000, 1:10000, 1:4000, 1:2000 and 1:1000) in PBS of the human serum of COVID-19 positive and negative cases. The electrode was immersed for 30 min into each solution with different dilution factors. Before the EIS analysis, the electrode was washed by immersion in PBS for 5 min and it was moved for a clean PBS for EIS measurements. The reproducibility was tested by evaluating distinct electrodes, synthesized using the same methodology, in one same positive and negative serum (n = 4). Also, a total of 10 clinical samples were evaluated by independent electrodes in 1:10000 dilution factor solutions; six samples were obtained from COVID-19 confirmed cases from hospitalized patients who had been diagnosed with SARS-CoV-2 infection by qRT-PCR by the Secretary of Health of the Paraná State.

3. Results and discussion

3.1. Modified electrode synthesis and characterization

PPy:PSS/AuNPs and PPy-NTs/AuNPs modified electrodes were characterized by SEM images, as shown if Fig. 1 (a) and (b), respectively. The images of the polymers without AuNPs can be found in. For PPy:PSS, the characteristic globular morphology of PPy was obtained [32], while nanotubes were randomly deposited at the stainless-steel mesh in the synthesis using MO as a template for polymerization [17]. In both cases, the presence of AuNPs is not verified in the secondary electron (SE) images; however, the back scattered electron images and EDS spectra of the electrodes confirmed the presence of Au in the materials (andFig. S2). The PPy:PSS film can also be visualized in the STEM image (Fig. 1 (c)), where the small black dots correspond to the AuNPs. Additionally, an EDS mapping image of PPy:PSS/AuNPs can be visualized inFig. S3, evidencing the AuNPs distribution along the material. The same black dots can be seen in the TEM image for PPy-NTs (Fig. 2 (d)), indicating the deposition of the AuNPs all over the nanotubes.

The amount of AuNPs was estimated as 2.98×10^{-4} cm^{-2} ($\pm 2.16 \times 10^{-4}$ cm^{-2}) for PPy:PSS, covering an area of 4.3% (±1%) of the polymer. For PPy-NTs, the amount of AuNPs was estimated as 3.18×10^{-4} cm^{-2} ($\pm 8.62 \times 10^{-5}$ cm^{-2}), covering an area of 4.30% (±0.4%). The higher standard deviation of PPy:PSS in relation to PPy-NTs is due to the lower resolution of STEM in comparison with TEM technique. The mean diameter of the AuNPs was estimated as 11 ± 3 nm for both materials.

The modified electrodes were characterized by cyclic voltammetry, as can be seen in Fig. 3 for (a) PPy:PSS and PPy:PSS/AuNPs and for (b) PPy-NTs and PPy-NTs/AuNPs. The PPy characteristic redox processes can be observed in CVs of (a) and (b), however, for PPy-NTs these processes appear in less energetic potentials, indicating a better charge transfer process in the nanotube morphology. Also, the presence of a polyelectrolyte on PPy:PSS/AuNPs material might change the whole ionic intercalation process inside/outside the polymeric matrix. These factors might have been contributed to different CV profiles for the film when compared to the nanotubular PPy. In the presence of AuNPs, both voltammograms show a current increase, probably due to the higher electroactive area. Also, a new

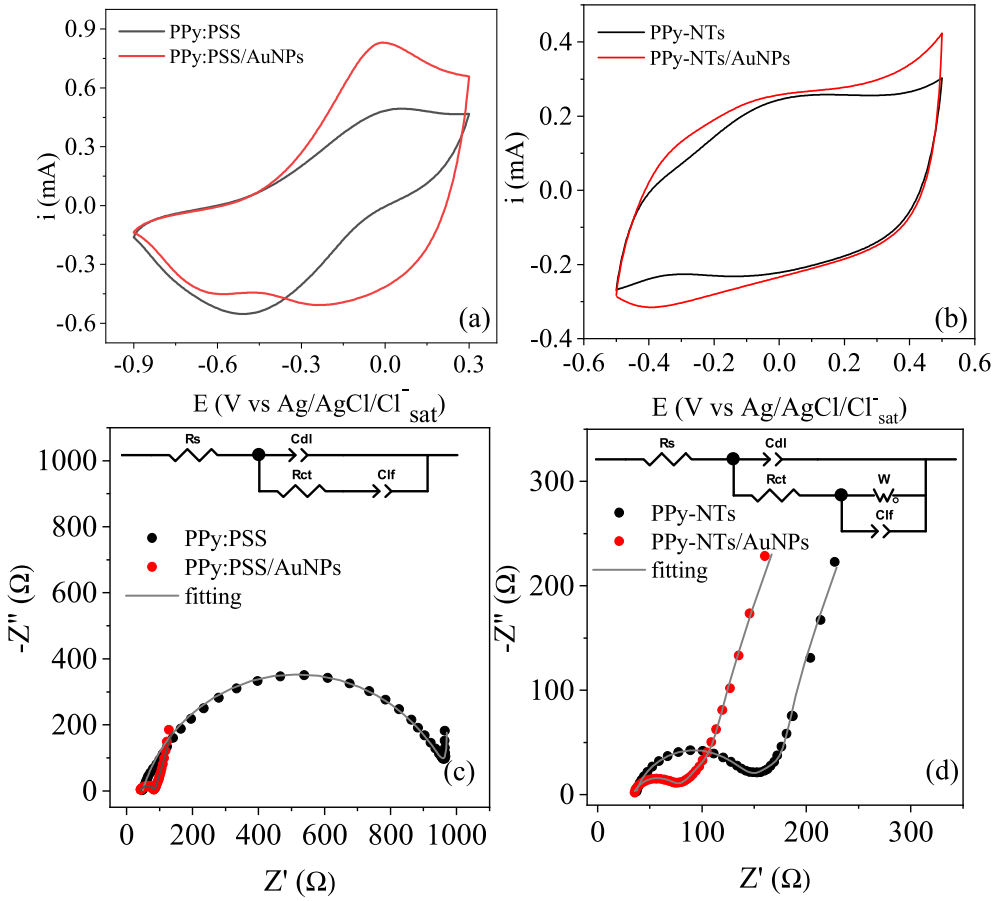

Fig. 3. CV of (**a**) PPy:PSS and (**b**) PPy-NTs at 20 mV/s in PBS. Nyquist diagrams of (**c**) PPy:PSS and (**d**) PPy-NTs at ocp in PBS. Inset: equivalent circuits used to fit the EIS data. EIS, electrochemical impedance spectroscopy; NT, nanotube; PBS, phosphate-buffered saline; PPy, polypyrrole.

reduction process appears for both PPy:PSS/AuNPs and PPy-NTs/AuNPs, indicating that the presence of metallic nanoparticles is leading to a different doping state of the polymer.

Nyquist diagram of PPy:PSS and PPy-NTs EIS measurements in the absence and presence of AuNPs are both shown in Fig. 3 (c) and (d), respectively. PPy:PSS EIS data were fitted using a Randles-modified equivalent circuit (inset in Fig. 3 (c)), a very well-established equivalent circuit for CPs modified electrodes [33,34]. In this equivalent circuit, *Rs* is the series resistance, accounting for the resistance of the electrolyte, connections and electrodes, *Rct* is the charge-transfer resistance, related to the charge transfer processes at the material/electrolyte interface, *Cdl* is a constant-phase element (CPE) describing the double layer capacitance and *ndl* is a parameter that is related to the double layer homogeneity, thus, depicting the material morphology, it can vary from 0 to 1, being the unity a perfect flat electrode representation. Another CPE is present, *Clf*, that is related to the charge intercalation process at the polymeric film to maintain electroneutrality upon the redox processes and *nlf*, that refers to this intercalation process homogeneity. For a better fitting of PPy-NTs and PPy-NTs/AuNPs EIS data, a Warburg element was inserted at the equivalent circuit, which is related to ionic diffusion in the polymer [34,35]. The calculated parameters are shown in Table 1.

The changes in *Rs* values can be assigned to a small variation in the constant cell each time a new measurement was carried out, in this way, it is difficult to readily interpret this data. For both polymers, *Cdl* increased in the materials with AuNPs, indicating a higher electroactive area thanks to nanoparticles present. This value is higher for PPy:PSS than PPy-NTs due to the former higher charge of deposition, probably owing a higher electroactive area. Also, after AuNPs deposition, a decrease in the *ndl* is verified, which can be related to a less homogenous interface. PPy:PSS showed a higher *Rct* than PPy-NTs due to the higher deposition charge and the presence of an insulating polymer in the composition (PSS). However, the *Rct* value has significantly decreased after AuNPs deposition for both polymers, indicating a more electroactive interface in the presence of the metallic nanoparticles. *Clf* also showed an increase in the presence of AuNPs for PPy:PSS, which may indicate that the nanoparticles are creating more electroactive sites, also increasing the number of intercalated ions. For this polymer, *nlf* was calculated as 0.99 which indicated a very homogeneous intercalation process inside the polymeric film. However, it has decreased in the presence of AuNPs, probably owing to a more heterogeneous distribution of AuNPs in the film, changing the oxidated or partially oxidated areas for intercalation. For PPy-NTs, the *Clf* was the same with and without the AuNPs evidencing the same number of intercalated ions, which probably is already close to the limit for this material due to the nanotube morphology; however, the decrease in the *nlf* shows a less homogeneous intercalation process in the presence of the AuNPs. The Warburg coefficient (σ) decreased in the presence of AuNPs, indicating a lower resistance for the diffusion, probably due to the improvement of redox process in the presence of AuNPs and, consequently, in the ionic diffusion.

3.2. COVID-19 biosensor construction characterization

The steps of electrode modification are schematized in Fig. 4 (a), where PPy is a representation of the two different morphologies (PPy:PSS or PPy-NTs). Each step of the modification was characterized by FTIR spectra, as shown in Fig. 4 (b) for PPy:PSS/AuNPs and (c) for PPy-NTs/AuNPs. In the spectrum of PPy:PSS/AuNPs, some pyrrole characteristic bands can be identified, as the broad band between 3,000 and 3,300/cm (Fig. S4) related to C–H and C–H stretching vibrations, at 1,448/cm assigned to the conjugated C–N stretching [36], 1,168 and 894, which correspond to the breathing of pyrrole and in plane C–H deformation, respectively, at 1,058/cm assigned to C–C out of plane deformation and a weak absorption at 673/cm [37], related to C–H out of plane bending of pyrrole. Some PSS bands are also visible, as the band at 1,635/cm, attributed to the water molecules associated with PSS via hydrogen bonding [37] and at 1,377/cm, related to R–SO_3 vibration [38]. PPy-NTs Fourier-transform infrared spectrum also showed PPy characteristic bands, as the broad band from 3,000 to 3,300/cm (Fig. S4), in 1,554 and 1,460/cm which are considered to be the result of N–H and C–H stretching vibrations, pyrrole ring stretches and conjugated C–N stretching, respectively [36], and the bands at 1,180 and 924/cm, indicating the doping state of PPy [39]. Some methyl orange bands can also be observed in the spectrum of PPy-NTs, as the bands at 1,400/cm, which is assigned to –CH_3 vibrations and at 1,035/cm, related to the asymmetric stretching vibration of –SO_3Na group [40].

The presence of MPA can be evidenced by the band at 3,450/cm (COOH vibration,Fig. S4), the enhancement of the band at 1,635/cm, assigned to C=O bonds of MPA [41] and the appearance of the bands at 1,377 and 1,554/cm (for PPy-NTs) and 1,398 and 1,550/cm (for PPy-PSS), for symmetric and asymmetric carboxylate stretching vibration, respectively [42]. The absence of a band at 2,600-2,500/cm at the MPA spectrum indicates that S–H is bounded at the Au surface [43]. The band at 1,550/cm disappeared after the N-protein immobilization, which evidences that EDC/NHS reaction and further N-protein covalent attachment was efficient.

After the blockage step, BSA bands are not evident in the spectrum due to the overlapping with other bands, but some signals can be verified as in 1,398/cm related to carboxylate groups and at 1,310/cm assigned to amide-III vibration. The electrodes were immersed in a solution containing the mAb anti N-protein to verify the antigen/antibody interaction. In the spectrum obtained after mAb interaction, the band at 1,554/cm for PPy-NTs reappeared. This band was observed before for other antigen-antibody complexes [44], indicating that the monoclonal antibody was properly attached at the biosensor surface. Also, the disappearance of the band at 1,635/cm may indicate that the mAb is interacting with the carbonyl group of N-protein.

The biosensor construction was electrochemically characterized by the CV (Fig. S5) where a diminishment of the total current is observed after each modification step, evidencing a more difficult charge transfer and/or charge intercalation processes in the presence of macromolecules. To better understand the changes seen by the CVs, EIS was performed after each modification step for PPy:PSS/AuNPs (Fig. 4 (d)) and PPy-NTs/AuNPs (Fig. 4 (e)). EIS data were adjusted with the equivalent circuits shown in Fig. 3 (c) and (d) for PPy:PSS/AuNPs and PPy-NTs/AuNPs, respectively, and the calculated parameters are present inTable S1.

As commented before, *Rs* values cannot be properly discussed due to small variations in the constant cell in each measurement.

Table 1
Parameters obtained through fitting EIS data present in Fig. 3.

Modified electrode	Rs/Ω	Cdl/μF s^{n-1}	ndl	Rct/Ω	Clf/mF s^{n-1}	nlf	σ/Ω $s^{-1/2}$
PPy:PSS	48.85	63.07	0.82	935.2	20.0	0.99	–
PPy:PSS/AuNPs	40.00	100.6	0.72	44.82	137.2	0.82	–
PPy-NTs	36.34	24.5	0.84	106.8	6.60	0.85	111.6
PPy-NTs/AuNPs	34.05	54.95	0.77	43.8	5.97	0.78	91.41

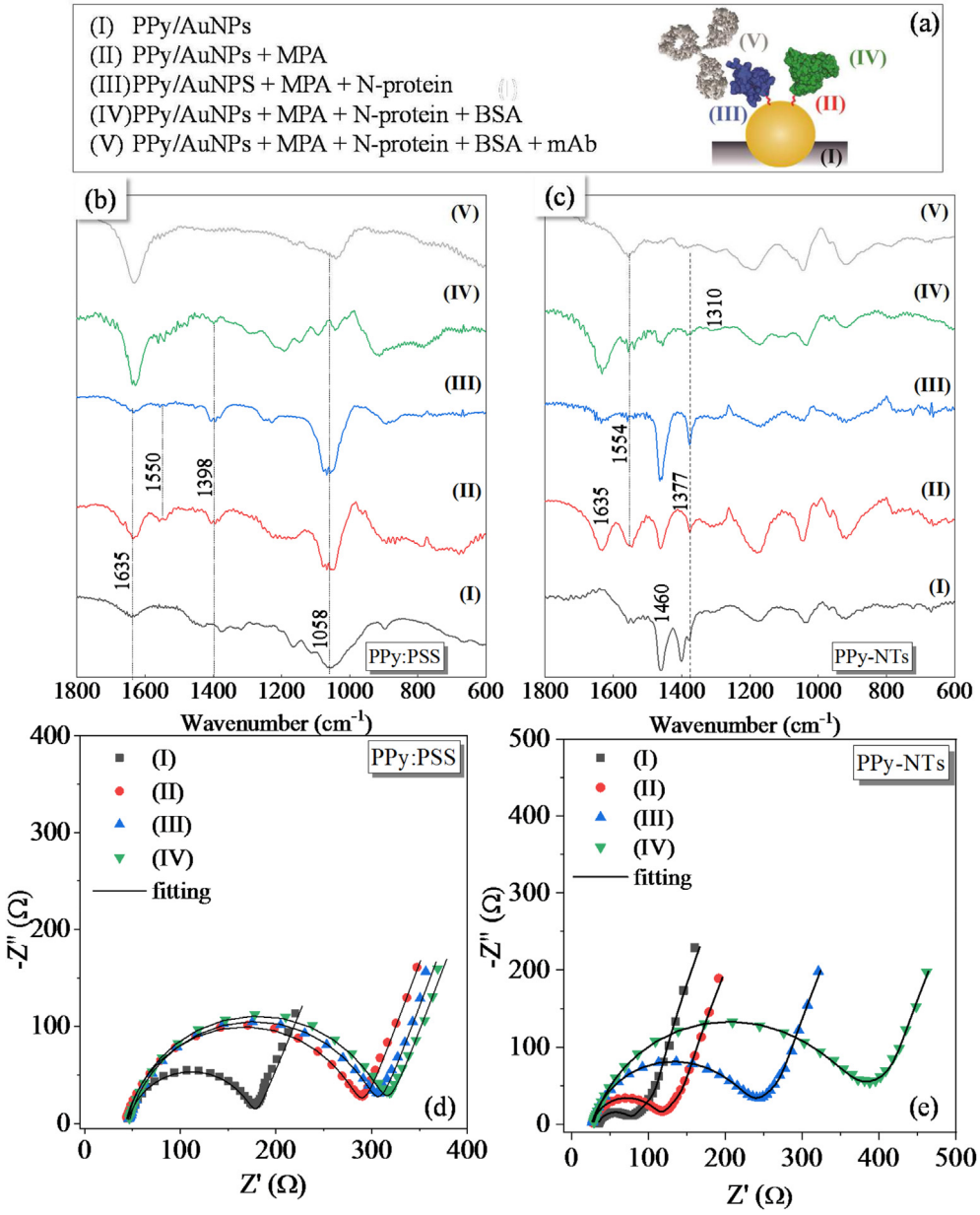

Fig. 4. (**a**) Schematic representation of each step for the biosensor construction. FT-IR of (**b**) PPy:PSS and (**c**) PPy-NTs and Nyquist diagrams of (**d**) PPy:PSS and (**e**) PPy-NTs after each modification step. FT-IR, Fourier-transform infrared spectroscopy; NT, nanotube; PPy, polypyrrole.

For both PPy:PSS and PPy-NTs, a decrease in the *Cdl* values after each modification step is observed, indicating that the exposed electroactive area is becoming smaller with the immobilizations at the electrode surface. Also, the *Rct* values increased after each modification step, indicating that the electrode/electrolyte interface is being blocked by the modifiers. For both materials, *Clf* values did not show a significant variation during the biosensor construction, indicating that the intercalation process in the polymeric matrix is not changed by the immobilizations. For PPy-NTs, the σ values increased with each modification step, indicating that the insulating molecules and macromolecules are blocking the electrode surface, hindering the ionic diffusion inside the polymer. EIS analysis in the presence of mAb will be discussed in the analytical evaluation (next section).

3.3. COVID-19 biosensor analytical evaluation

The response for both PPy morphologies to different concentrations of a monoclonal SARS-CoV-2 antibody was compared using EIS, and the respective calibration plots can be found in Fig. 5.

The Nyquist diagrams present in Fig. 5 (a),(c) exhibit the respective biosensors response to different concentrations of purified anti N-protein monoclonal antibody. The EIS data were fitted considering the equivalent circuits shown in Fig. 3 (c) and (d) for PPy:PSS/AuNPs and PPy-NTs/AuNPs, respectively. The electrochemical parameter that presented reasonable alterations by antigen-antibody interaction was the *Rct*, evidenced by enlargement of the semi-circle diameter in the higher frequency region. This change is related to the insulating structures increase on the

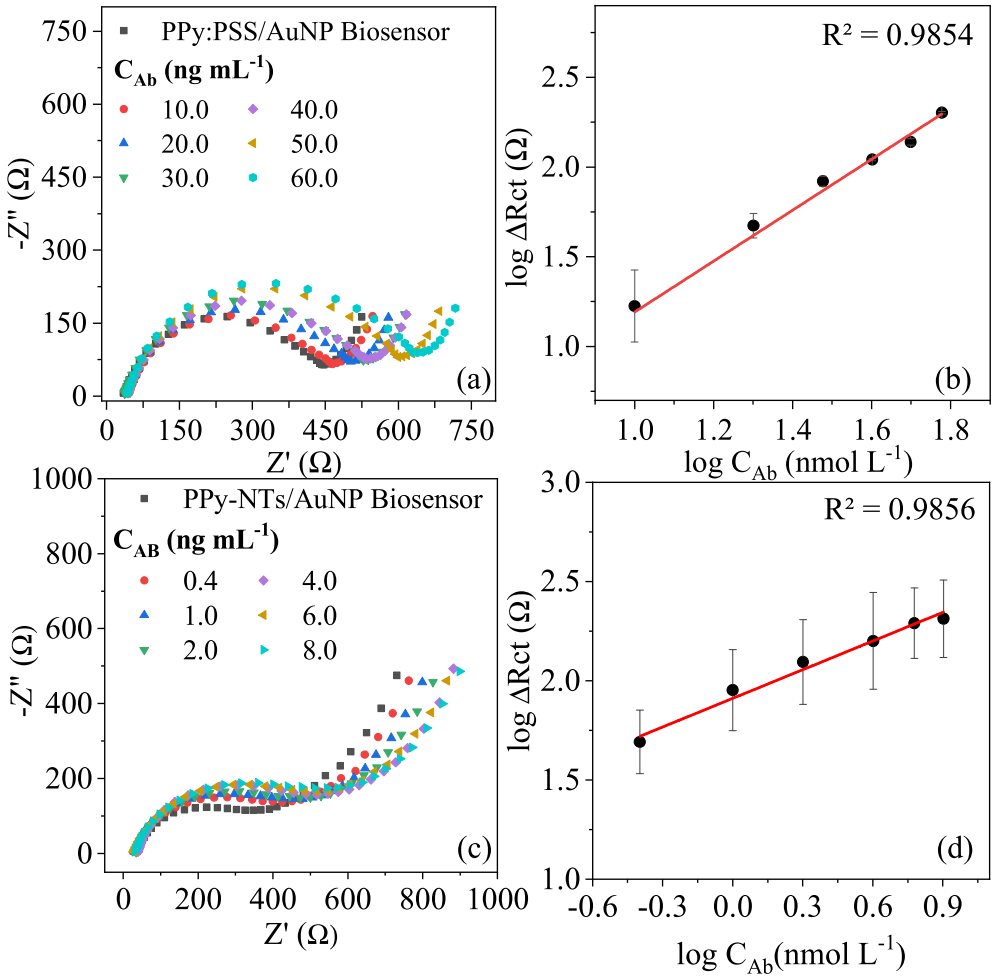

Fig. 5. Nyquist diagrams of (**a**) PPy:PSS and (**b**) PPy-NTs biosensors exposed to different concentrations of anti N-protein IgG antibody obtained in PBS at OCP and the linear response between these logarithmic concentrations and the logarithmic of *ΔRct* for (**c**) PPy-NTs (**d**) PPy:PSS. NT, nanotube; PPy, polypyrrole.

electrode surface due to their affinity with the recognition unity previously immobilized onto this surface, forming an immunocomplex antigen-antibody that impair the charge transfer between the bulk and the polymer [13]. *ΔRct* was chosen to construct the calibration plot to minimize the influence of the initial *Rct*, which might be different due to the inevitable variability in area delimitation, polymer synthesis, and biomolecules attachment in each biosensor construction experiment. A linear correlation between the logarithmic *ΔRct* and the logarithmic mAb concentration can be found in Fig. 5 (b) and (d) to the PPy:PSS/AuNPs from 10 to 60 ng/mL and PPy-NTs/AuNPs from 0.4 to 8 ng/mL, respectively, showing that the N-protein was successfully immobilized onto both electrode surface.

The PPy-NTs higher surface area promoted a better biosensor detectability, presenting a limit of detection (LOD) of 0.386 ng/mL and limit of quantification (LOQ) of 1.287 ng/mL against LOD = 2.456 ng/mL and LOQ = 7.442 ng/mL for the PPy:PSS film, calculated by considering LOD = 3 × SD/m and LOQ = 10 × SD/m (where *SD* is the standard derivation of 10 electrode's EIS measurements prior to monoclonal antibody exposure and *m* is sensibility). However, from the calibration plot, the LOQ for PPy-NTs/AuNPs can be considered the lowest concentration in the linear range, 0.4 ng/mL. Considering sensibility, the angular coefficient was mathematically transformed to allow comparison between both calibrations. PPy-NTs presented a sensibility nine times higher than PPy:PSS ($m = 32.03\ \Omega$ mL/ng vs. $m = 3.55\ \Omega$ mL/ng), even with a lower N-protein concentration immobilized onto the sensor surface and smaller charge of deposition, showing that the higher surface area improved the electrode analytical properties.

Among electrochemical biosensors available up to this day in the literature, there are a few works using EIS as a transducer [45–51], although just one impedimetric biosensor for antibody detection in serum samples. Rashed et al. presented a very fast impedance sensing platform to detect SARS-CoV-2 antibodies in serum specimens, testing concentrations of 0.1, 1.0 and 10 μg mL. This platform was able to differentiate positive and negatives patient serums, showing consistency when compared to enzyme-linked immunosorbent assay test results, using a spike protein receptor-binding domain (SP RBD) as bioreceptor [45]. Among other electrochemical biosensors, Yakoh et al. [52]produced a paper-based and label-free platform for diagnosing COVID-19, utilizing a redox probe, which when in presence of the specific antibodies, interrupted the redox conversion, causing a decrease in current response (detected by square-wave voltammetry). This work used as recognition unity SP RBD and presented LOQ of 1 ng/mL (evaluated for IgG and IgA). More recently, Rahmati et al. [53] developed a sensitive electrochemical biosensor immobilizing spike protein in nickel hydroxide nanoparticles, utilizing screen-printed carbon electrode as a platform, showing a LOD of 0.3 fg/mL for antibody detection (IgG/IgM).

The PPy-NTs/AuNPs biosensor produced by this work conferred remarkable sensibility, allowing the antibodies detection in PBS, without the necessity of an electrochemical probe, using a small quantity of the bioreceptor (N-protein) and deposited in a significantly affordable material (stainless-steel mesh), which can be disposable, favoring a low-cost measurement.

However, the inaccuracy of serological tests can be a challenge [54], requesting a better sensitivity allied to an efficient selectivity to avoid false positives. Since the PPy-NTs/AuNPs electrode showed improved sensibility, this morphology was selected to evaluate the device ability to separate negative from positive serum in real samples.

3.4. Detection of SARS-CoV-2 seroconversion in clinical samples

The PPy-NTs/AuNPs biosensor response (evaluated by *ΔRct* as discussed previously) in face of different dilutions of serum samples obtained from hospitalized COVID-19 positive patients or negative samples can be found in Fig. 6 (a). Nyquist diagrams for biosensor exposition to different dilutions of one positive and one negative serum sample is displayed inFig. S6. It is possible to observe a reproducible difference in response of both serums, even in highly diluted samples. SARS-CoV-2 antibodies present in the positive sample that are absent in the negative sample, specifically interact with the bioreceptor, block the interface and consequently interfere in the charge transference process, increasing its resistance, as showed before using the monoclonal mAb solutions. In contrast, the use of negative real samples is important to obtain the biosensor selectivity since serum corresponds to a complex matrix composed by water, inorganic compounds, and many lipids and proteins, with antibodies that recognize different antigens.

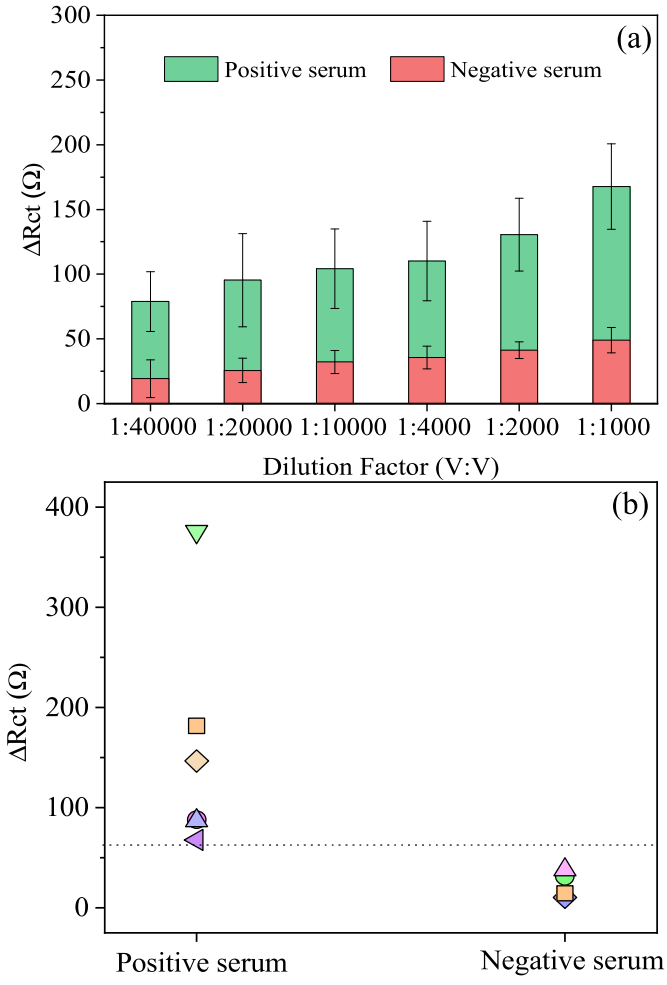

Fig. 6. (**a**) Reproducibility (n = 4) of PPy-NTs/AuNPs immunosensor for an individual positive serum versus a negative response in different dilution factors (V:V) and (b) several (n = 10) confirmed positive and negative samples discriminated by their EIS response in a 1:10000 dilution factor.

However, because serum is complex matrix, and the immunological response to SARS-CoV-2 infections varies in the population, it is important to consider that each sample may behave differently. For that reason, other serum samples of different positive and negative cases were tested (n = 6 and n = 4, respectively), using 1:10000 dilution factor in PBS since at this dilution, it was possible to observe on average a 3-fold increment of the *ΔRct* value when comparing positive/negative response. In Fig. 6 (b) is placed the different samples analyzed, being able to separate the COVID-19 positive cases from the negatives. To discriminate the results, it was calculated an optimal cut-off value (positive/negative threshold) based on the test results from uninfected samples, by adding the average (x) negative individual samples response by 3x their standard deviation (*cut-off* = x + 3 × SD) [55]. The PPy-NTs/AuNPs platform successfully separated all the serums samples tested.

4. Conclusion

The screening of SARS-CoV-2 antibodies is essential for the infection control. Even though many studies have been focusing on the electrochemical biosensors development, the creation of a simple and disposable platform, without the need of redox probes is still a big challenge. In this context, this work compared two different PPy morphologies, PPy:PSS and PPy-NTs, characterized by electrochemical, spectroscopical, and microscopical techniques. Both polymeric morphologies embedded with gold nanoparticles provided ideal platforms to protein attachment and further antibody sensing, quantifying 7.442 and 0.4 ng/mL for PPy:PSS and PPy-NTs, respectively. Hence, the nanostructured polymer PPy-NTs presented almost eight times higher sensibility than the globular morphology, showing an improvement of the platform when utilizing a nanostructured surface, being this platform selected to further explore its bioanalytical ability in real samples. The novel impedimetric biosensing platform rapidly (in less than 1 h) and sensitively detected specific antibodies presence in human serums and showed up to be a flexible, probe-free and disposable. In addition, a small volume is used to produce the biosensor response, being promising to further finger prick blood tests development. This low-cost system can be prospected for COVID-19 immunosurveillance, as well as a small volume with further modifications can be used for infection screening or even vaccination effectivity in producing antibodies. Some limitations as the stability, which was not tested herein, the number of steps required for the bioreceptor immobilization, and the sample preparation should be explored in future works.

Credit author statement

Bruna M. Hryniewicz: Conceptualization, Methodology, Validation, Investigation, Writing - Original Draft, **Jaqueline Volpe:** Conceptualization, Methodology, Validation, Investigation, Writing - Original Draft, **Larissa Bach-Toledo:** Conceptualization, Methodology, Validation, Investigation, Writing - Original Draft, **Kamila C. Kurpel:** Investigation, **Andrei E. Deller:** Investigation, **Ana Leticia Soares:** Investigation, **Jeanine M. Nardin:** Resources, **Luís F. Marchesi:** Conceptualization, Validation, **Fernanda F. Simas:** Conceptualization, Methodology, Validation, Writing - Review &

Editing, **Carolina C. Oliveira:** Conceptualization, Methodology, Validation, Resources, Writing - Review & Editing, **Luciano Huergo:** Conceptualization, Methodology, Validation, **Dênio E. P. Souto:** Conceptualization, Methodology, Validation, Writing - Review & Editing, Supervision, Project administration, **Marcio Vidotti:** Conceptualization, Methodology, Validation, Resources, Writing - Review & Editing, Supervision, Project administration, Funding acquisition.

Funding

This work was suported by Alexander von Humboldt Foundation, UFPR-Proind. This study was financed in part by the Coordenação de Aperfeiçoamento de Pessoal de Nível Superior - Brasil (CAPES) – Finance Code 001.

Declaration of competing interest

The authors declare that they have no known competing financial interests or personal relationships that could have appeared to influence the work reported in this article.

Acknowledgements

The authors gratefully acknowledge CTI Renato Archer and Centro de Microscopia Eletrônica da UFPR (CME-UFPR) for microscopic facilities and the financial support from UTFPR (Edital 4K), CNPq (303038/2019-5 and 408635/2018-5), INCT in Bioanalytics (FAPESP grant no. 2014/50867-3 and CNPq grant no. 465389/2014-7).

Appendix A. Supplementary data

Supplementary data to this article can be found online at https://doi.org/10.1016/j.mtchem.2022.100817.

References

[1] W. Guan, Z. Ni, Y. Hu, W. Liang, C. Ou, J. He, L. Liu, H. Shan, C. Lei, D.S.C. Hui, B. Du, L. Li, G. Zeng, K.-Y. Yuen, R. Chen, C. Tang, T. Wang, P. Chen, J. Xiang, S. Li, J. Wang, Z. Liang, Y. Peng, L. Wei, Y. Liu, Y. Hu, P. Peng, J. Wang, J. Liu, Z. Chen, G. Li, Z. Zheng, S. Qiu, J. Luo, C. Ye, S. Zhu, N. Zhong, Clinical characteristics of coronavirus disease 2019 in China, N. Engl. J. Med. 382 (2020) 1708–1720, https://doi.org/10.1056/nejmoa2002032.

[2] M. Yüce, E. Filiztekin, K.G. Özkaya, COVID-19 diagnosis —a review of current methods, Biosens. Bioelectron. 172 (2021) 112752, https://doi.org/10.1016/j.bios.2020.112752.

[3] P. Pokhrel, C. Hu, H. Mao, Detecting the coronavirus (COVID-19), ACS Sens. 5 (2020) 2283–2296, https://doi.org/10.1021/acssensors.0c01153.

[4] F. Cui, H.S. Zhou, Diagnostic methods and potential portable biosensors for coronavirus disease 2019, Biosens. Bioelectron. 165 (2020) 112349, https://doi.org/10.1016/j.bios.2020.112349.

[5] E. Morales-Narváez, C. Dincer, The impact of biosensing in a pandemic outbreak: COVID-19, Biosens. Bioelectron. 163 (2020) 112274, https://doi.org/10.1016/j.bios.2020.112274.

[6] A. Bonanni, M. Del Valle, Use of nanomaterials for impedimetric DNA sensors: a review, Anal. Chim. Acta 678 (2010) 7–17, https://doi.org/10.1016/j.aca.2010.08.022.

[7] E. Cesewski, B.N. Johnson, Electrochemical biosensors for pathogen detection, Biosens. Bioelectron. 159 (2020) 112214, https://doi.org/10.1016/j.bios.2020.112214.

[8] L. Xia, Z. Wei, M. Wan, Conducting polymer nanostructures and their application in biosensors, J. Colloid Interface Sci. 341 (2010) 1–11, https://doi.org/10.1016/j.jcis.2009.09.029.

[9] M.H. Naveen, N.G. Gurudatt, Y.B. Shim, Applications of conducting polymer composites to electrochemical sensors: a review, Appl. Mater. Today 9 (2017) 419–433, https://doi.org/10.1016/j.apmt.2017.09.001.

[10] M. Gerard, A. Chaubey, B.D. Malhotra, Application of conducting polymers to biosensors, Biosens. Bioelectron. 17 (2001) 345–359.

[11] V. Van Tran, N.H.T. Tran, H.S. Hwang, M. Chang, Development strategies of conducting polymer-based electrochemical biosensors for virus biomarkers: potential for rapid COVID-19 detection, Biosens. Bioelectron. 182 (2021) 113192, https://doi.org/10.1016/j.bios.2021.113192.

[12] A. Bogomolova, E. Komarova, K. Reber, T. Gerasimov, O. Yavuz, S. Bhatt, M. Aldissi, Challenges of electrochemical impedance spectroscopy in protein biosensing, Anal. Chem. 81 (2009) 3944–3949, https://doi.org/10.1021/ac9002358.

[13] M.I. Prodromidis, Impedimetric immunosensors—a review, Electrochim. Acta 55 (2010) 4227–4233, https://doi.org/10.1016/j.electacta.2009.01.081.

[14] A. Sargent, O.A. Sadik, Monitoring antibody–antigen reactions at conducting polymer-based immunosensors using impedance spectroscopy, Electrochim. Acta 44 (1999) 4667–4675, https://doi.org/10.1016/S0013-4686(99)00265-0.

[15] B.M. Hryniewicz, L. Bach-Toledo, M. Vidotti, Harnessing energy from micropollutants electrocatalysis in a high-performance supercapacitor based on PEDOT nanotubes, Appl. Mater. Today 18 (2020), https://doi.org/10.1016/j.apmt.2019.100538.

[16] A.L. Soares, B.M. Hryniewicz, A.E. Deller, J. Volpe, L.F. Marchesi, D.E.P. Souto, M. Vidotti, Electrodes based on PEDOT nanotubes decorated with gold nanoparticles for biosensing and energy storage, ACS Appl. Nano Mater. 4 (2021) 9945–9956, https://doi.org/10.1021/acsanm.1c02677.

[17] B.M. Hryniewicz, R.V. Lima, F. Wolfart, M. Vidotti, Influence of the pH on the electrochemical synthesis of polypyrrole nanotubes and the supercapacitive performance evaluation, Electrochim. Acta 293 (2019) 447–457, https://doi.org/10.1016/j.electacta.2018.09.200.

[18] A. Sharma, A. Kumar, Study of structural and electro-catalytic behaviour of amperometric biosensor based on chitosan/polypyrrole nanotubes-gold nanoparticles nanocomposites, Synth. Met. 220 (2016) 551–559, https://doi.org/10.1016/j.synthmet.2016.07.012.

[19] E.N. Zare, T. Agarwal, A. Zarepour, F. Pinelli, A. Zarrabi, F. Rossi, M. Ashrafizadeh, A. Maleki, M.A. Shahbazi, T.K. Maiti, R.S. Varma, F.R. Tay, M.R. Hamblin, V. Mattoli, P. Makvandi, Electroconductive multi-functional polypyrrole composites for biomedical applications, Appl. Mater. Today 24 (2021) 101117, https://doi.org/10.1016/j.apmt.2021.101117.

[20] X. Song, J. Mei, G. Ye, L. Wang, A. Ananth, L. Yu, X. Qiu, In situ pPy-modification of chitosan porous membrane from mussel shell as a cardiac patch to repair myocardial infarction, Appl. Mater. Today 15 (2019) 87–99, https://doi.org/10.1016/j.apmt.2019.01.003.

[21] M. Lin, A dopamine electrochemical sensor based on gold nanoparticles/over-oxidized polypyrrole nanotube composite arrays, RSC Adv. 5 (2015) 9848–9851, https://doi.org/10.1039/C4RA14360D.

[22] E.B. Aydın, Highly sensitive impedimetric immunosensor for determination of interleukin 6 as a cancer biomarker by using conjugated polymer containing epoxy side groups modified disposable ITO electrode, Talanta 215 (2020) 120909, https://doi.org/10.1016/j.talanta.2020.120909.

[23] K. Xue, S. Zhou, H. Shi, X. Feng, H. Xin, W. Song, A novel amperometric glucose biosensor based on ternary gold nanoparticles/polypyrrole/reduced graphene oxide nanocomposite, Sensor. Actuator. B Chem. 203 (2014) 412–416, https://doi.org/10.1016/j.snb.2014.07.018.

[24] J.C. Love, L.A. Estroff, J.K. Kriebel, R.G. Nuzzo, G.M. Whitesides, Self-assembled monolayers of thiolates on metals as a form of nanotechnology, Chem. Rev. 105 (2005) 1103–1169, https://doi.org/10.1021/cr0300789.

[25] D.E.P. Souto, A.M. Fonseca, J.T.C. Barragan, R. de C.S. Luz, H.M. Andrade, F.S. Damos, L.T. Kubota, SPR analysis of the interaction between a recombinant protein of unknown function in Leishmania infantum immobilised on dendrimers and antibodies of the visceral leishmaniasis: a potential use in immunodiagnosis, Biosens. Bioelectron. 70 (2015) 275–281, https://doi.org/10.1016/j.bios.2015.03.034.

[26] D.E.P. Souto, J.V. Silva, H.R. Martins, A.B. Reis, R.C.S.S. Luz, L.T. Kubota, F.S.F.S. Damos, Development of a label-free immunosensor based on surface plasmon resonance technique for the detection of anti-Leishmania infantum antibodies in canine serum, Biosens. Bioelectron. 46 (2013) 22–29, https://doi.org/10.1016/j.bios.2013.01.067.

[27] L.F. Huergo, K.A. Selim, M.S. Conzentino, E.C.M. Gerhardt, A.R.S. Santos, B. Wagner, J.T. Alford, N. Deobald, F.O. Pedrosa, E.M. De Souza, M.B. Nogueira, S.M. Raboni, D. Souto, F.G.M. Rego, D.L. Zanette, M.N. Aoki, J.M. Nardin, B. Fornazari, H.M.P. Morales, V.A. Borges, A. Nelde, J.S. Walz, M. Becker, N. Schneiderhan-Marra, U. Rothbauer, R.A. Reis, K. Forchhammer, Magnetic bead-based immunoassay allows rapid, inexpensive, and quantitative detection of human SARS-CoV-2 antibodies, ACS Sens. 6 (2021) 703–708, https://doi.org/10.1021/acssensors.0c02544.

[28] M. Naseri, L. Fotouhi, A. Ehsani, Recent progress in the development of conducting polymer-based nanocomposites for electrochemical biosensors applications: a mini-review, Chem. Rec. 18 (2018) 599–618, https://doi.org/10.1002/tcr.201700101.

[29] H. Yamato, M. Ohwa, W. Wernet, Stability of polypyrrole and poly(3,4-ethylenedioxythiophene) for biosensor application, J. Electroanal. Chem. 397 (1995) 163–170, https://doi.org/10.1016/0022-0728(95)04156-8.

[30] T. Kremers, M. Tintelott, V. Pachauri, X.T. Vu, S. Ingebrandt, U. Schnakenberg, Microelectrode combinations of gold and polypyrrole enable highly stable two-electrode electrochemical Impedance spectroscopy measurements under turbulent flow conditions, Electroanalysis 33 (2021) 197–207, https://doi.org/10.1002/elan.202060105.

[31] A.L. Soares, M.L. Zamora, L.F. Marchesi, M. Vidotti, Adsorption of catechol onto PEDOT films doped with gold nanoparticles: electrochemical and spectroscopic studies, Electrochim. Acta 322 (2019) 134773, https://doi.org/10.1016/j.electacta.2019.134773.

[32] X. Cui, J.F. Hetke, J.A. Wiler, D.J. Anderson, D.C. Martin, Electrochemical deposition and characterization of conducting polymer polypyrrole/PSS on

multichannel neural probes, Sens. Actuators A Phys. 93 (2001) 8–18, https://doi.org/10.1016/S0924-4247(01)00637-9.
[33] L.F. Marchesi, S.C. Jacumasso, R.C. Quintanilha, H. Winnischofer, M. Vidotti, The electrochemical impedance spectroscopy behavior of poly(aniline) nanocomposite electrodes modified by Layer-by-Layer deposition, Electrochim. Acta 174 (2015) 864–870, https://doi.org/10.1016/j.electacta.2015.05.077.
[34] W.A. Gazotti, T. Matencio, M.-A. De Paoli, Electrochemical impedance spectroscopy studies for chemically prepared poly(o-methoxyaniline) doped with functionalized acids, Electrochim. Acta 43 (1998) 457–464, https://doi.org/10.1016/S0013-4686(97)00120-5.
[35] B.W. Johnson, D.C. Read, P. Christensen, A. Hamnett, R.D. Armstrong, Impedance characteristics of conducting polythiophene films, J. Electroanal. Chem. 364 (1994) 103–109, https://doi.org/10.1016/0022-0728(93)02923-6.
[36] J. Jang, H. Yoon, Facile fabrication of polypyrrole nanotubes using reverse microemulsion polymerization, Chem. Commun. 3 (2003) 720–721, https://doi.org/10.1039/b211716a.
[37] S. Maruthamuthu, J. Chandrasekaran, D. Manoharan, R. Magesh, Conductivity and dielectric analysis of nanocolloidal polypyrrole particles functionalized with higher weight percentage of poly(styrene sulfonate) using the dispersion polymerization method, J. Polym. Eng. 37 (2017) 481–492, https://doi.org/10.1515/polyeng-2015-0321.
[38] M.J. González-Tejera, M.A. La De Plaza, E. De Sánchez La Blanca, I. Hernández-Fuentes, Electrochemical, FTIR and morphological study of polypyrrole—polystyrenesulphonate conducting films, Polym. Int. 31 (1993) 45–50, https://doi.org/10.1002/pi.4990310108.
[39] X. Zhang, J. Zhang, Z. Liu, C. Robinson, Inorganic/organic mesostructure directed synthesis of wire/ribbon-like polypyrrole nanostructures, Chem. Commun. (2004) 1852–1853, https://doi.org/10.1039/b405255b.
[40] P. Li, Y. Song, S. Wang, Z. Tao, S. Yu, Y. Liu, Enhanced decolorization of methyl orange using zero-valent copper nanoparticles under assistance of hydrodynamic cavitation, Ultrason. Sonochem. 22 (2015) 132–138, https://doi.org/10.1016/j.ultsonch.2014.05.025.
[41] S.R. Ankireddy, J. Kim, Dopamine-functionalized inp/zns quantum dots as fluorescence probes for the detection of adenosine in microfluidic chip, Int. J. Nanomed. 10 (2015) 121–128, https://doi.org/10.2147/IJN.S88465.
[42] R. Itteboina, U.Di Madhuri, P. Ghosal, M. Kannan, T.K. Sau, T. Tsukuda, S. Bhardwaj, Efficient one-pot synthesis and pH-dependent tuning of photoluminescence and stability of Au 18 (SC 2 H 4 CO 2 H) 14 cluster, J. Phys. Chem. A. 122 (2018) 1228–1234, https://doi.org/10.1021/acs.jpca.7b10888.
[43] A. de Bettencourt-Dias, R.A. Tigaa, Sensitization of near-infrared Ln III [Ln = Yb or Nd] ions using water-soluble, band gap tuneable 3-MPA-capped CdS nanoparticles, J. Mater. Chem. C. 6 (2018) 2814–2821, https://doi.org/10.1039/C7TC05821G.
[44] R. Barbucci, A. Magnani, C. Roncolini, S. Silvestri, Antigen-antibody recognition by Fourier transform IR spectroscopy/attenuated total reflection studies: biotin-avidin complex as an example, Biopolymers 31 (1991) 827–834, https://doi.org/10.1002/bip.360310703.
[45] M.Z. Rashed, J.A. Kopechek, M.C. Priddy, K.T. Hamorsky, K.E. Palmer, N. Mittal, J. Valdez, J. Flynn, S.J. Williams, Rapid detection of SARS-CoV-2 antibodies using electrochemical impedance-based detector, Biosens. Bioelectron. 171 (2021) 112709, https://doi.org/10.1016/j.bios.2020.112709.
[46] R.M. Torrente-Rodríguez, H. Lukas, J. Tu, J. Min, Y. Yang, C. Xu, H.B. Rossiter, W. Gao, SARS-CoV-2 RapidPlex: a graphene-based multiplexed telemedicine platform for rapid and low-cost COVID-19 diagnosis and monitoring, Matter 3 (2020) 1981–1998, https://doi.org/10.1016/j.matt.2020.09.027.
[47] M.A. Ehsan, S.A. Khan, A. Rehman, Screen-printed graphene/carbon electrodes on paper substrates as impedance sensors for detection of coronavirus in nasopharyngeal fluid samples, Diagnostics 11 (2021) 1030, https://doi.org/10.3390/diagnostics11061030.
[48] Z. Rahmati, M. Roushani, H. Hosseini, H. Choobin, Electrochemical immunosensor with Cu2O nanocube coating for detection of SARS-CoV-2 spike protein, Microchim. Acta 188 (2021), https://doi.org/10.1007/s00604-021-04762-9.
[49] M.D.T. Torres, W.R. Araujo, L.F. Lima, A. Ferreira, C. Fuente-Nunez, Low-cost biosensor for rapid detection of SARS-CoV-2 at the point of care, Matter 4 (2021) 2403–2416, https://doi.org/10.1016/j.matt.2021.05.003.
[50] V.J. Vezza, A. Butterworth, P. Lasserre, E.O. Blair, A. MacDonald, S. Hannah, C. Rinaldi, P.A. Hoskisson, A.C. Ward, A. Longmuir, S. Setford, E.C.W. Farmer, M.E. Murphy, D.K. Corrigan, An electrochemical SARS-CoV-2 biosensor inspired by glucose test strip manufacturing processes, Chem. Commun. 57 (2021) 3704–3707, https://doi.org/10.1039/d1cc00936b.
[51] E.B. Aydın, M. Aydın, M.K. Sezgintürk, Highly selective and sensitive sandwich immunosensor platform modified with MUA-capped GNPs for detection of spike Receptor Binding Domain protein: a precious marker of COVID 19 infection, Sensor. Actuator. B Chem. 345 (2021) 130355, https://doi.org/10.1016/j.snb.2021.130355.
[52] A. Yakoh, U. Pimpitak, S. Rengpipat, N. Hirankarn, O. Chailapakul, S. Chaiyo, Paper-based electrochemical biosensor for diagnosing COVID-19: detection of SARS-CoV-2 antibodies and antigen, Biosens. Bioelectron. 176 (2021) 112912, https://doi.org/10.1016/j.bios.2020.112912.
[53] Z. Rahmati, M. Roushani, H. Hosseini, H. Choobin, An electrochemical immunosensor using SARS-CoV-2 spike protein-nickel hydroxide nanoparticles bio-conjugate modified SPCE for ultrasensitive detection of SARS-CoV-2 antibodies, Microchem. J. 170 (2021) 106718, https://doi.org/10.1016/j.microc.2021.106718.
[54] G. Liu, J.F. Rusling, COVID-19 antibody tests and their limitations, ACS Sens. 6 (2021) 593–612, https://doi.org/10.1021/acssensors.0c02621.
[55] R.H. Jacobson, Validation of serological assays for diagnosis of infectious diseases, Rev. Sci. Tech. 17 (1998) 469–526, https://doi.org/10.20506/rst.17.2.1119.